ADVANCED MATERIALS INTERFACES
Open Access
www.advmatinterfaces.de

Investigation of the Few-Layer Black Phosphorus Degradation by the Photonic Measurements

Małgorzata Szczerska, Monika Kosowska, Jakub Gierowski, Mateusz Cieślik, Mirosław Sawczak, and Paweł Jakóbczyk**

Few-layer black phosphorus (FLBP) is a 2D material that gains worldwide interest for its possible applications, mainly in electronics and optoelectronics. However, as FLBP is prone to a degradation process under environmental conditions, there is a need for a monitoring method allowing investigation of its surface quality. Among many techniques, optoelectronic ones have unique advantages of fast response, non-contact, and non-invasive operation. In this paper, a photonic method is presented for this purpose with a focus on the earliest stages of the degradation process. Measurements are performed using a fiber-optic interferometer working at the wavelength of 1310 nm. Series of material characterization measurements, including scanning electron microscopy, X-ray photoelectron spectroscopy, and Raman spectroscopy investigations are performed to examine the FLBP using a well-established methodology. Two samples—with liquid exfoliated FLBP and with layers of supernatant—prepared in two different production processes are investigated over 3 h. A detailed presentation of the degradation process is provided. The results prove that the surface monitoring of FLBP is possible by registering optical signal changes correlated with the changes in optical parameters caused by the proceeding degradation process.

1. Introduction

The discovery of graphene in 2004 has started a worldwide interest in two-dimensional (2D) materials: extensive research on their development, characterization and potential applications is carried out. The set of optical and electrical parameters of the 2D materials motivates studies on their applications in, e.g., sensing,[1–4] flexible electronics,[5,6] detectors[7] and emitters,[8] photovoltaics,[9] supercapacitors,[10] and many more.[11–14] Among numerous 2D materials (like boron nitride, molybdenum disulfide, borophene, or a new class of 2D materials called MXenes,[15] discovered in 2011) we can distinguish single-layer black phosphorus (BP) called phosphorene.[16,17]

It has high-carrier mobility (up to 103 cm^2 Vs^{-1}),[18] a high on-off ratio (≈10^5 for monolayer),[19] and a refractive index of $n \approx 2.3–2.7$ (@1330 nm).[20] Black phosphorus direct bandgap is tuned by the number of layers and varies from 0.3 to 2 eV.[21] A puckered honeycomb structure of phosphorene is characterized by strong anisotropy. These properties make phosphorene a useful material for the development of elements such as photodetectors,[22] solar panels,[23] absorbers,[24] and linear polarizers.[25]

Although BP exhibits the aforementioned advantages, it degrades under environmental conditions.[26] Based on the literature studies,[27] the degradation process has two stages: oxidation of the phosphorene, and further reactions with water leading to acid formation. In the first step, chemical adsorption of oxygen and formation of dangling bonds occur, then a series of phosphorus oxides on the surface appear. The degradation process is especially rapid in the first hours, after the production of phosphorene, in contact with the ambient environment (oxygen, moisture). Wang et al.[28] report that during the first 4 h phosphorus oxide (P_2O_5) is formed, which blocks the surface and slows down the degradation process. The second step begins in

M. Szczerska, J. Gierowski, P. Jakóbczyk
Department of Metrology and Optoelectronics
Faculty of Electronics
Telecommunications and Informatics
Gdańsk University of Technology
11/12 Narutowicza Street, Gdańsk 80-233, Poland
E-mail: malszcze@pg.edu.pl; pawel.jakobczyk@pg.edu.pl

The ORCID identification number(s) for the author(s) of this article can be found under https://doi.org/10.1002/admi.202202289.

DOI: 10.1002/admi.202202289

M. Kosowska
Faculty of Telecommunications
Computer Science and Electrical Engineering
Bydgoszcz University of Science and Technology
Al. prof. S. Kaliskiego 7, Bydgoszcz 85-796, Poland

M. Cieślik
Institute of Nanotechnology and Materials Engineering
Division of Electrochemistry and Surface Physical Chemistry
Gdańsk University of Technology
11/12 Narutowicza Street, Gdańsk 80-233, Poland

M. Sawczak
Centre for Plasma and Laser Engineering
The Szewalski Institute of Fluid Flow Machinery
Fiszera 14 Street, Gdańsk 80-231, Poland

the next hours and days, as a result of the hygroscopic nature of the phosphorus oxide, dry phosphoric acid (H_3PO_4) and phosphorous acid (H_3PO_3) are formed.[29,30] It should be noted that unoxidized phosphorene, according to the results of simulations, does not react with H_2O—for this to occur, phosphorene must be oxidized first.[31] The formation of surface oxides promotes further degradation due to their exothermic reaction with water. It was shown that environmental factors like exposure to light and temperature can speed up the degradation of phosphorene.[32–34]

Improved and real-time evaluation of the quality of 2D material should help overcome the barriers that potentially hinder research and progress toward applications. Clearly, more information on phosphorene changes during research is desirable, especially at the early stage of aging, when the process progresses very quickly. The most important methods are atomic force microscopy (AFM),[28,33,35] transmission electron microscopy (TEM),[36] scanning electron microscopy (SEM),[37] Phosphorus-31 nuclear magnetic resonance (^{31}P NMR),[28] and Raman spectroscopy.[38,39] However, most of the methods used to assess the BP surface and its changes require sophisticated and expensive equipment. The monitoring is based on chemical analysis or visual subjective evaluation. Moreover, Raman spectroscopy or microscopy can reveal mostly long-term changes.

In this work, a fiber-optic interferometer was used to observe the degradation of freshly produced FLBP (few-layer black phosphorus) with a focus on the initial stage. This device is highly sensitive,[40–42] resistant to electromagnetic interferences,[43] moreover, its physical dimensions are small and the design is relatively simple, reducing the overall cost of implementation.[44] The interferometer allows observing changes in the optical signal in real-time.[43,45] If the system works under constant measurement conditions, changes in the optical signal result only from changes in the properties of the reflecting layer.[46] This allows monitoring of the chemical process dynamics via changes in absorption and refractive index.[47,48] Despite the undoubted advantages of this methodology, to date, it has not been used for FLBP degradation process investigation. This paper describes the measurement setup, experiments and results of FLBP monitoring by photonic measurements using the fiber optic interferometer.

2. Experimental Section

2.1. Few-Layer Black Phosphorus

Few-layer black phosphorus (FLBP) was prepared by solvent-assisted exfoliation from 35 mg pre-ground black phosphorus (BP, Smart Elements) dispersed in 8 mL of deoxygenated 95% ethanol (Sigma Aldrich) by purging with the highest purity class argon (Air Liquid). The BP dispersion was sonicated under an argon stream using a horn probe ultrasonicator (Bandelin Sonopuls HD2200, 20 kHz), where the temperature was maintained in the range from 0 to 3 °C with the use of an ice-cooled bath. The sonication tip was operated at 40 W power with a 0.5/0.5 s ON/OFF time for 4 h to break the van der Waals bonds in the BP crystal. The as-prepared suspension has been divided into two parts.

Table 1. Sample naming convention.

Sample A	Sample with liquid exfoliated FLBP (without centrifugation)
Sample B	Sample with layers of supernatant (with centrifugation)

One part was centrifuged at 6000 rpm for 15 min to remove the residual unexfoliated BP, yielding supernatant. Supernatant and liquid exfoliated FLBP (without centrifugation) were used for the spin coating of the silicon substrate. The silicon (Si) substrate was treated by the rolling circle amplification (RCA) process to clean its surface. The 20 µL of the supernatant and exfoliated BP without centrifugation were applied on the Si wafer. Then, the sample was rotated at a speed of up to 1000 rpm for 30 s using a spin coater. The procedure was repeated 7 times, and as a result, the FLBP layer was deposited on the Si substrate from an FLBP solution with a total volume of 140 µL. The sample naming convention was presented in **Table 1**.

2.2. Deposited FLBP Layers Characterization

In order to provide reference measurements for the presented method, the prepared samples were characterized by well-established methodology in the field. Characterization of the samples was performed using X-Ray Photoelectron Spectroscopy (XPS), Raman Spectroscopy and Field Emission Scanning Electron Microscopy.

XPS studies were carried out using Escalab 250Xi (ThermoFisher Scientific), utilizing AlKα X-ray spot with a diameter of 500 µm. The procedure applied was explained in detail elsewhere.[49] Adventitious carbon C1s (284.6 eV) was used for the peak calibration.

The FLBP coating was characterized by a Raman spectrometer. The Raman spectra were recorded by a confocal micro-Raman spectrometer (InVia, Renishaw, United Kingdom) with a 532 nm excitation laser (Ar ion laser) operating at 1% of its total power (50 mW). The Raman shift was in the range of 300–550 cm^{-1}.

The morphology and distribution of FLBP on the surface were characterized by the Schottky field emission scanning electron microscopy (Quanta FEG 250, FEI, USA) with ET secondary electron detector. The beam accelerating voltage was kept at 20 kV.

2.3. Photonic Measurement Setup

The measurement setup was constructed as a fiber optic interferometer working in a reflective mode. A 1310 nm light source (SLD-1310-18-W, FiberLabs Inc., Japan) was used in this study. The light was guided through the single-mode optical fibers (SMF-28, Thorlabs, USA). The measurement head was created by the polished fiber optic end-face placed above the reflective surface—measured FLBP sample. The two parallel surfaces constituted an interferometric cavity which transfer function can be described by a two-beam approximation. The incident light splits on the first surface, partially reflecting back and

ADVANCED MATERIALS INTERFACES
Open Access
www.advmatinterfaces.de

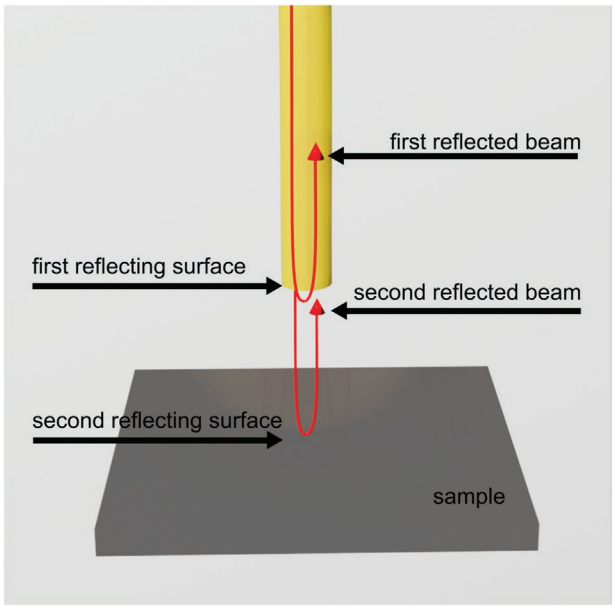

Figure 1. Measurement head operation principle. The interfering beams reflected from the fiber end–face/air interface and air/sample interface are transmitted back through the fiber to the detector.

partially transmitting. The transmitted light travels through the cavity and reflects back on the second reflective surface (**Figure 1**).

The two reflected beams interfere giving a resultant measurement signal recorded by an optical spectrum analyzer (OSA—Ando AQ6319, Tokyo, Japan). Changes occurring within the cavity lead to optical signal modulation. The measurement setup parameters are presented in **Table 2**.

The schema of the experimental setup is presented in **Figure 2**.

The registered optical signal contains information about the parameters of the sample: its absorption and refractive index.[50]

Table 2. Measurement setup parameters.

Parameter	Value
OSA resolution band	0.1 nm
OSA dynamic range	60 dB
Light source bandwidth	≥52 nm
Light source power	≥ 18 mW
Light source wavelength	1310 ± 20 nm
Light source full-width at half maximum [FWHM]	108 nm

The degradation process of the FLBP causes the fluctuations of the optical parameters of the sample, such as refractive index and absorption, which can be detected by the tracking the changes in the measured spectra. The proposed optical method is able to detect these changes and a fast, real time monitoring set-up of dynamic sample changes can be performed.

3. Results and Discussion

3.1. Morphology Analysis of FLBP Layers

The morphology differences between the prepared sample layers were performed by scanning electron microscopy. Noticeable differences between the samples can be observed in the SEM images presented in **Figure 3**a–h. Dark spots around flakes are due to water adsorption, phosphorene decomposition, formation H_3PO_4 and H_3PO_3 and subsequent drying. For sample B already at time 0 (Figure 3c,d) degradation effects are visible due to temporary exposure to air and moisture during sample preparation for SEM measurement. After 24 h (Figure 3e–h), the spots are larger, some of the flakes have completely disappeared, and only the larger ones remain. With flakes of greater thickness (Sample A), the process is slower and less visible on SEM images.

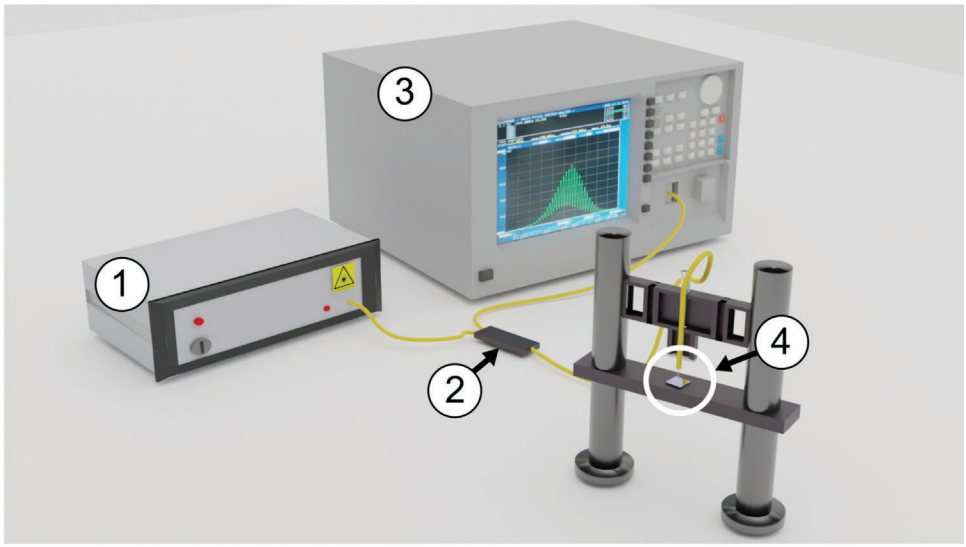

Figure 2. Measurement setup: 1—light source, 2—fiber-optic coupler, 3—optical spectrum analyzer, 4—measurement head placed in the micromechanical setup.

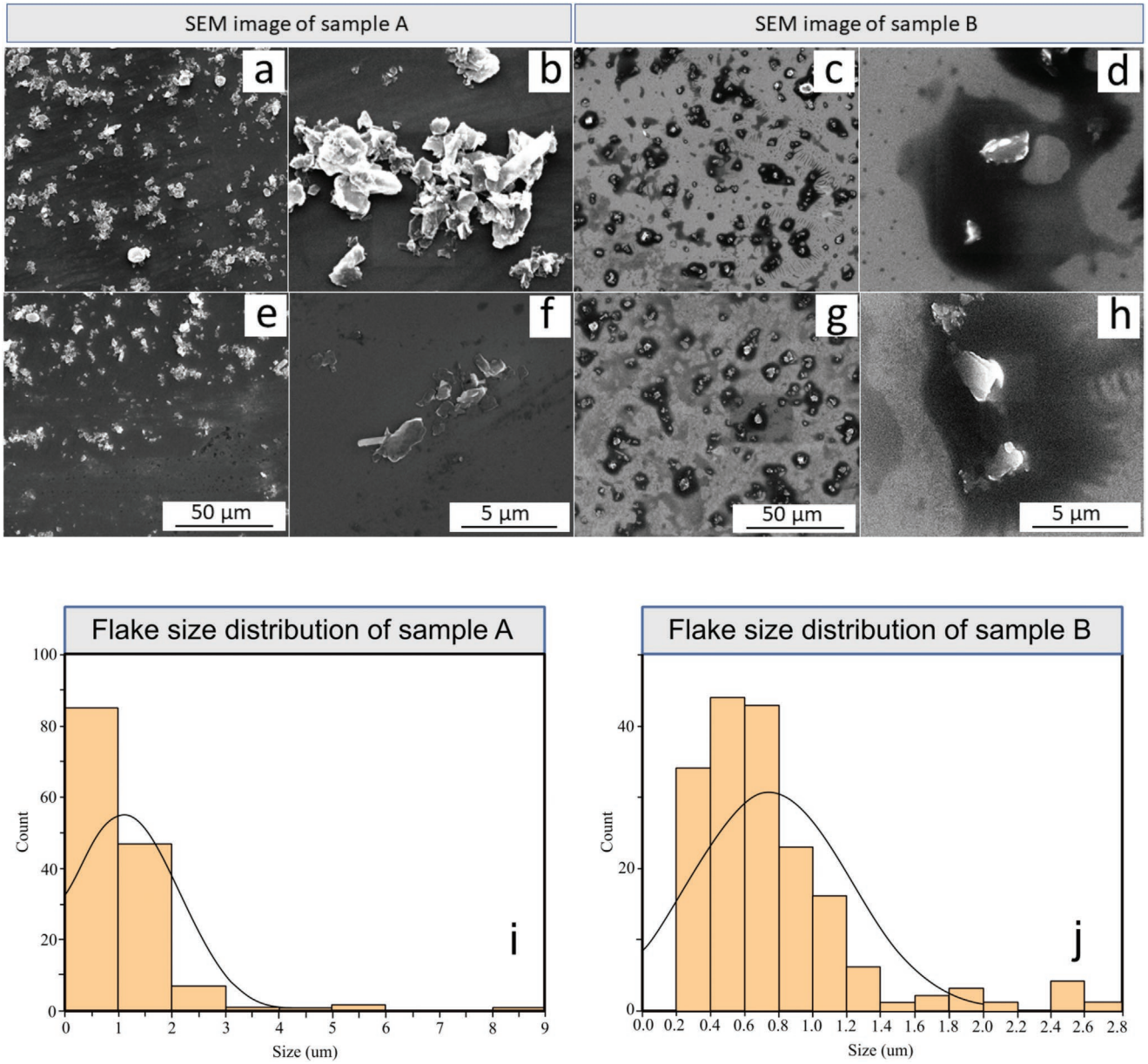

Figure 3. SEM measurements: a,b) SEM image of sample A in 0 time, c,d) SEM image of sample B in 0 time; e,f) SEM image of sample A after 24 h exposure in ambient conditions and g,h) SEM image of sample B after 24 h exposure in ambient conditions. i) Flake size distribution of sample A; j) flake size distribution of sample B. Sample A is the sample with liquid exfoliated FLBP (without centrifugation), and sample B is the sample with layers of supernatant.

Sample A has significantly larger particles of phosphorus flakes on the surface than sample B, which can be confirmed by the statistical distribution. Greater particles appearing could be agglomerates of many smaller flakes. Figure 3i,j shows the flake size distribution for investigated samples. For sample A, the largest number of flakes was counted for 1 µm, the other significant group of flakes is those with a size of 1–2 µm. The distribution of flake size for sample B is different, the majority lies in the range <1 µm. The two largest groups are those with a size of 0.4–0.6 and 0.6–0.8 µm. The centrifugation process significantly influenced the size of the flakes on the surfaces.

The surface of the FLBP layer is non-uniform, its thickness depends on the arrangement of the flakes. Based on SEM images, the layer thickness values for sample A ranged from 660 to 2.42 µm, and the average thickness was 1.28 µm. The thickness of Sample B was from 170 to 315 nm, and the average thickness was equal to 240 nm.

Thanks to the use of centrifugation during the preparation of sample B, not only the diameter of the flakes decreased, but also the thickness of the layer formed on the surface of the silicon substrate. The average thickness of the sample was determined by averaging the thickness of 6 locations in two cross-section SEM images of the sample (**Figure 4**).

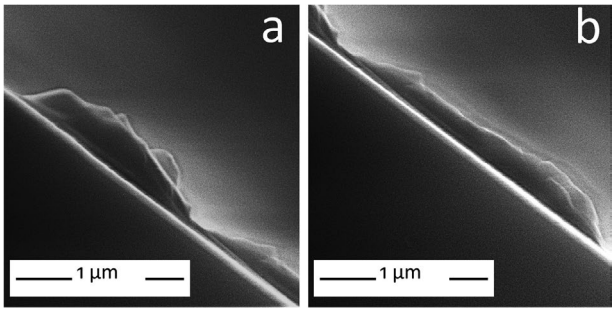

Figure 4. Scanning electron microscopy study of few-layer black phosphorus flakes. a,b) Images of a layer of black phosphorus flakes on a silicon substrate—cross-section of sample B.

3.2. XPS Surface Chemistry Analysis of FLBP

The XPS analyses reveal a significant difference in the surface chemical composition of the samples depending on the fabrication procedure. **Figure 5** shows the P2p binding energy range XPS spectra.

For sample B, the phosphorous is primarily gone from the surface, with some P_2O_5 remnants.[51]

On the other hand, for sample A, a strong peak doublet, with $P2p_{3/2}$ at 130.1 eV was observed. The energy range is characteristic of phosphorene,[52] also previously reported by our group.[49] It should be noted that both of these samples were kept in Ar atmosphere, and were only exposed to air during transport and mounting at the spectroscope. Nevertheless, the time appears to be sufficient for partial phosphorene oxidation, with several oxidation forms emerging and identified as P-O-P and O-P = O.[52] The share composition of each phosphorous moiety was summarized in **Table 3**.

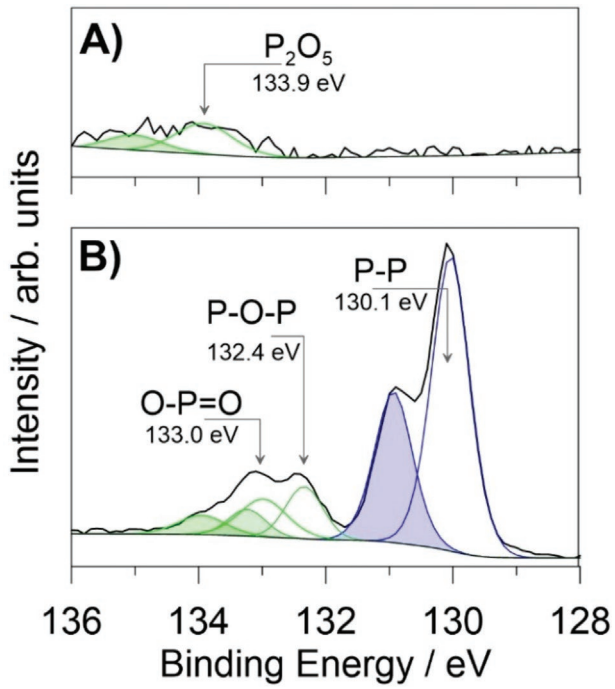

Figure 5. The P2p XPS spectra of the studied sample with the proposed deconvolution mode.

Table 3. Surface chemical composition of FLBP coatings based on XPS analysis.

Sample	P-P 130.1 eV	P-O-P 132.4 eV	O-P = O 133.0 eV	P_2O_5 133.9 eV
Sample A	74%	12%	14%	–
Sample B	–	–	–	100%

3.3. Raman Analysis during Degradation of FLBP

FLBP was first observed in ambient conditions at different aging times using Raman spectroscopy (**Figure 6**a) to see its stability. In Raman spectra, there are three peaks at about 359, 437, and 464 cm^{-1} corresponding to the three vibration modes A_g^1, A_g^2, and B_g^2.[50,53,54] After FLBP preparation (aging time 0), FLBP had a peak A_g^1 higher than A_g^2, but within the first 3 h a change is noticeable and the A_g^1/A_g^2 intensity ratio is below 1. A_g^1/A_g^2 ratio intensity of the Raman peaks reduces with time (Figure 5b) and confirms the instability of FLBP in the ambient environment.[55]

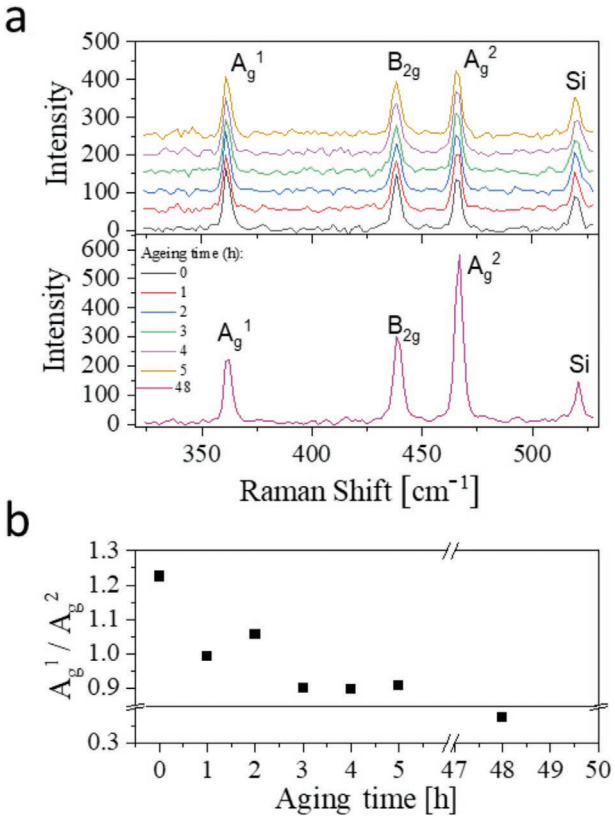

Figure 6. a) Raman spectra and b) the Raman A_g^1/A_g^2 intensity ratio of FLBP after different aging time.

ADVANCED MATERIALS INTERFACES
Open Access
www.advmatinterfaces.de

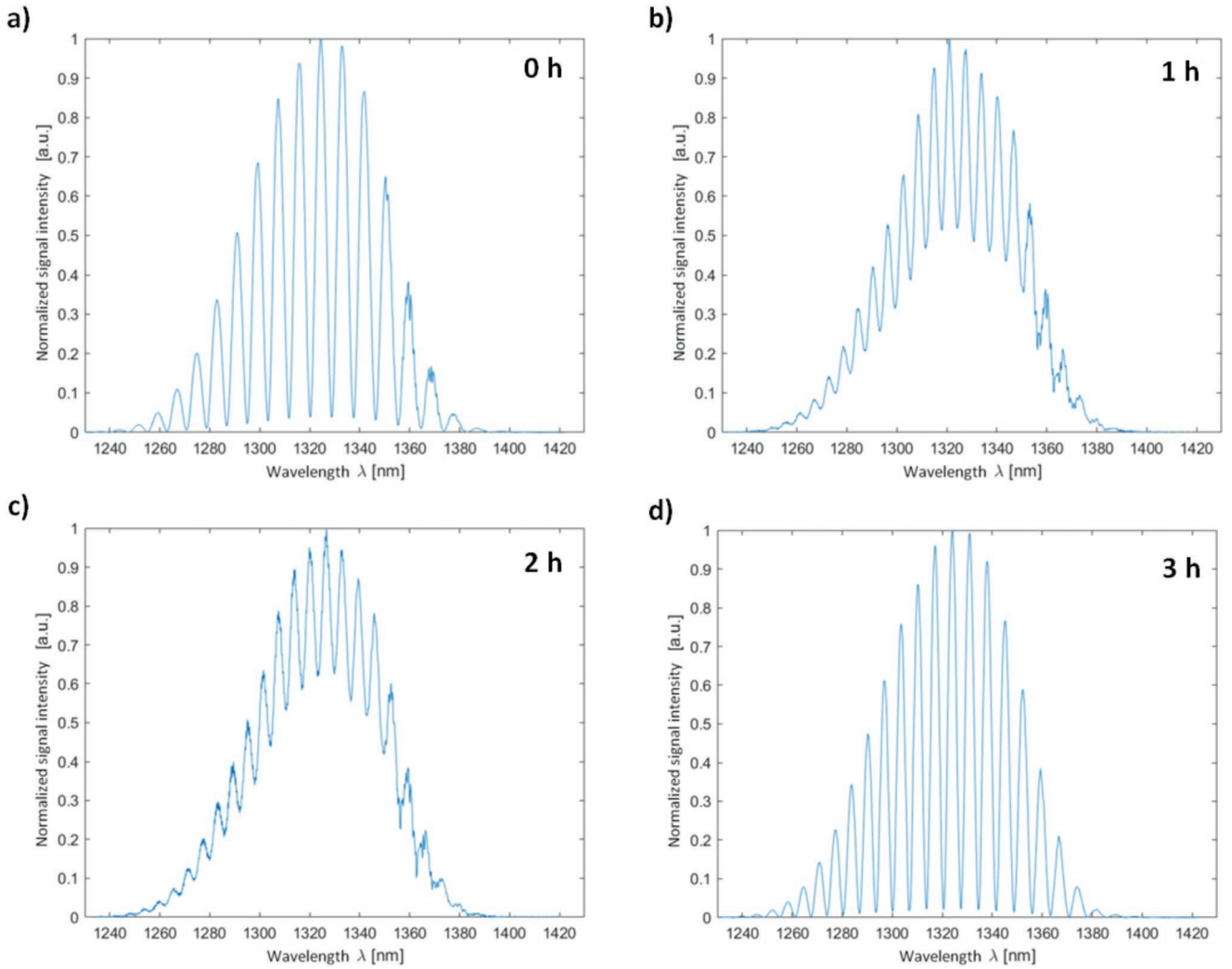

Figure 7. Normalized optical spectra of sample A (FLBP without centrifugation) after a) 0 h, b) 1 h, c) 2 h, d) 3 h after film preparation.

3.4. Photonic Measurements

The optical investigation was performed for both samples—spectra were recorded immediately after sample preparation (0 h), then after 1 h, 2 h, and 3 h. Interval time measurements allow observation of changes in optical properties caused by the degradation process of the samples. In the presented methodology, the optical signal visibility is considered as a parameter describing the proceeding degradation process. It is possible to track changes occurring in the FLBP sample via investigation of the measured signal visibility value because it is dependent on the reflectivity of the surface. The reflectivity is directly connected with refractive index.[56] Therefore, information about signal visibility allows us to conclude about the progressing degradation process, that changes sample refractive index due to changes in the chemical structure. The measured signal visibility can reach a maximum of 1, where an optical spectrum shows good contrast manifested through clearly distinguishable peaks. The lower the signal visibility, the worse contrast and the more difficult or even impossible differentiation of maxima in the spectrum. Visibility is defined as follows:[57]

$$V = \frac{I_{max} - I_{min}}{I_{max} + I_{min}} \quad (1)$$

where I_{max} is the maximum intensity in the optical spectrum and I_{min} is the minimum value neighboring to the peak with maximum intensity. **Figure 7** shows normalized optical spectra taken for sample A in its central point.

The optical spectra changed over time. After 1 h since sample preparation, the optical spectra show a significant drop in signal visibility. The worsening of this parameter can be attributed to the absorption increase indicating changes in the optical properties of the sample. This may be the effect of the formation of an oxide layer on the surface, as well as hydroxide ions (OH^-) that exhibit high absorption in the considered wavelength range.[58,59] Significant changes in the measured sample surface after 1 h are following the results of Koenig et al.[60] An increase in the FLBP surface roughness was observed with

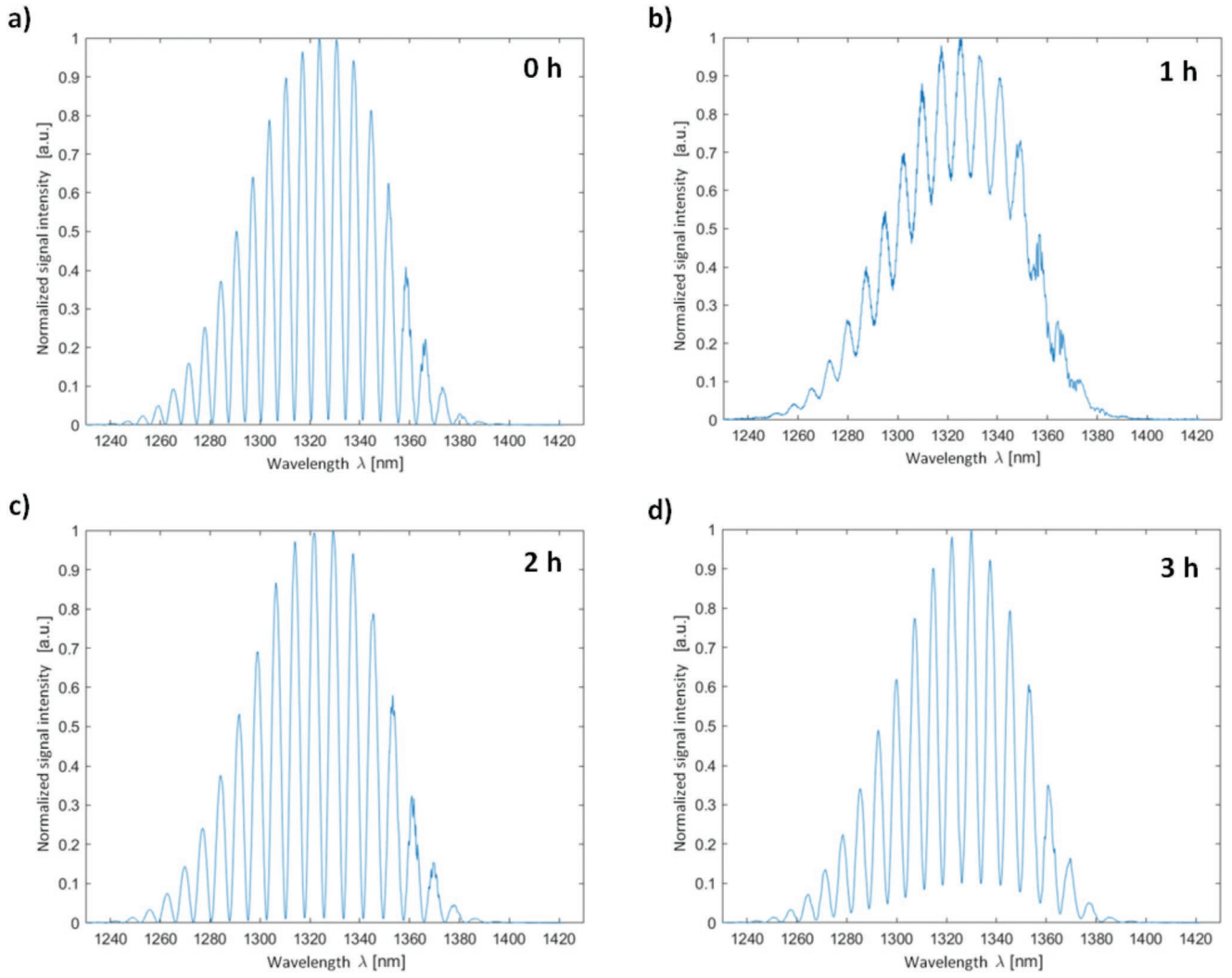

Figure 8. Normalized optical spectra of sample B (FLBP with centrifugation) after a) 0 h, b) 1 h, c) 2 h, d) 3 h, after film preparation.

AFM, showing rapid oxidation over a short time. Analogical measurements were taken at the central point of Sample B, **Figure 8** presents acquired optical spectra.

Sample B presents the same behavior, changes in optical parameters are occurring with time. There is a significant signal visibility drop registered after the first hour from sample preparation indicating the fast-progressing aging process appearing shortly after sample preparation.

Changes in the modulation of the spectra indicate dynamic chemical changes in the prepared samples. **Figure 9** presents the visibility of the measured signals plotted as a function of time.

The initial signal visibility for both samples is comparable, showing good surface quality. The degradation process is the most rapid in the first hour of exposing samples to environmental conditions, and a significant drop appears. However, after 1 h, the signal visibility for Sample A is higher than for the Sample B. It can be attributed to a small amount of phosphorus and the presence of more decomposition products for

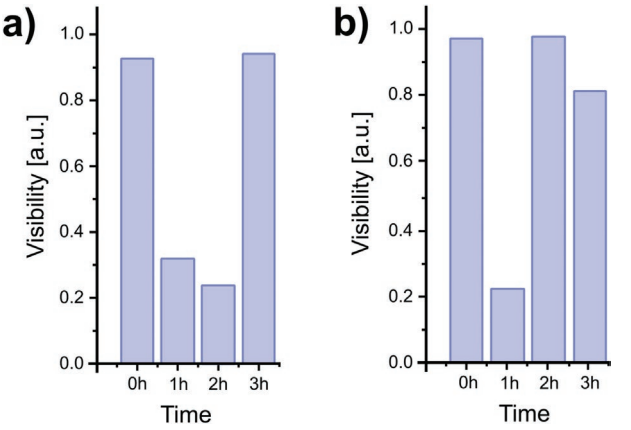

Figure 9. Time-varying interferometric signal visibility for few-layer black phosphorus a) sample A—without centrifugation and b) sample B—with centrifugation.

ADVANCED MATERIALS INTERFACES
Open Access
www.advmatinterfaces.de

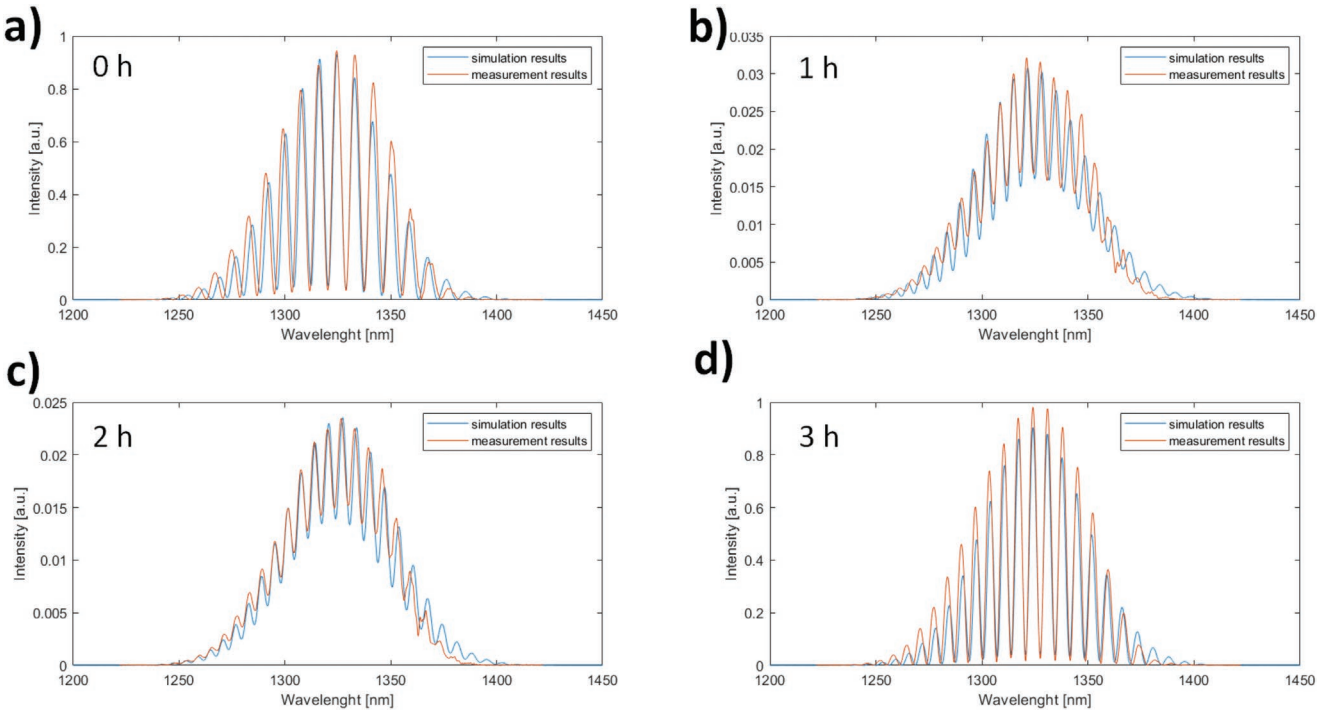

Figure 10. Comparison of the simulation and measurement results for Sample A after: a) 0 h, b) 1 h, c) 2 h, d) 3 h.

the latter, which is in agreement with XPS and Raman results. Progressing degradation of both samples results in higher visibility values of the measured signals which can be explained by the significant impact of the substrate on the reflection of light. As the absorption values of FLBP change over time, which is an effect of long-term exposure to environmental conditions, the acquired signal modulation and the fluctuations of signal visibility values[61] appear, proving the correct operation of the proposed photonic sensor.

The results of the performed experiments were compared with computer simulations. A model of a two-beam interferometer was implemented, following the experimental setup of the measurement head. The calculations were based on the Fresnel equations for each interface between different optical media. Simulated results are presented in the form of signal spectra on the output of the system, assuming ideal Gaussian shaped spectrum of the light source. A series of simulations were made to find values of signal absorption and cavity refractive index that gave the most similar results to the measured ones in terms of signal intensity and visibility. Theoretical and measured signals are shown in **Figures 10** and **11**.

It can be noted that the signals registered during experiments follow theoretical modeling as there is a satisfying fit between the results: the corresponding maxima are in agreement and overlap. Hence, the model is correct enabling estimation of absorption and refractive index in the cavity. Final values of estimated parameters are shown in **Tables 4** and **5**.

The obtained values show that the absorption significantly rises during the sample degradation. As mentioned before, layer absorption increase can be explained by the formation of phosphorus oxides reacting with H_2O and forming phosphorus acid. In both cases, the absorption value exceeds 0.9 and drops after 3 h for sample A, and after 2 h for sample B as a result of their degradation. As the estimated refractive index tends to the value characteristic for water, it can be concluded that oxygen and hydrogen molecules are present in the cavity, confirming formation of phosphorus acid with progressing degradation of FLBP.

4. Conclusions

A fiber-optic interferometer was used to observe changes in optical spectra during the FLBP degradation process. A light source operating at the wavelength of 1310 nm was used as a high OH^- absorption appears in this region, increasing the system's sensitivity to FLBP surface degradation. The study included two samples, differing in the preparation method. Optical measurements were performed within 3 h during which FLBP was exposed to environmental conditions. Changes in optical parameters within the initial stage of the degradation process were registered: the value of signal visibility was alternated due to changes occurring in the measured sample, indicating progressive degradation. The measurement and theoretical results were compared showing high agreement, that enabled optical parameters estimation. Well-established methodology for chemical analysis was used to provide a reference and present the FLBP degradation process in detail. Series of material characterization investigations, including SEM, XPS, and Raman spectroscopy. The progressing degradation of both samples was presented. The sample prepared in the process with centrifugation exhibited faster phosphorus decomposition.

The experiments have shown that assessment of FLBP surface is possible using a photonic method, advantageous to

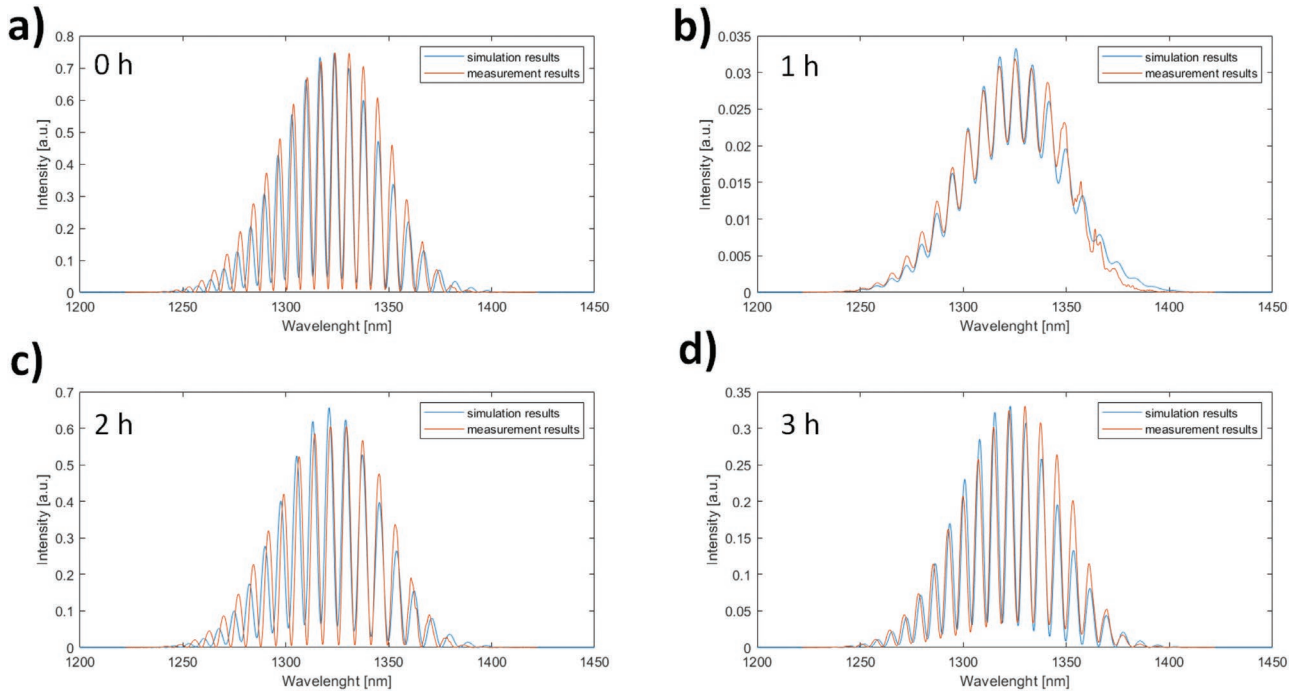

Figure 11. Comparison of the simulation and measurement results for Sample B after: a) 0 h, b) 1 h, c) 2 h, d) 3 h.

Table 4. Optical parameters estimated for sample A.

Time [h]	Absorption	Refractive index in the cavity
0	0	1
1	0.9	1.26
2	0.92	1.28
3	0	1

Table 5. Optical parameters estimated for sample B.

Time [h]	Absorption	Refractive index in the cavity
0	0	1.05
1	0.965	1.245
2	0.1	1.1
3	0.325	1.2

Table 6. Comparison of measurement methods.

Method	Analysis	Ref.
Fiber-optic interferometer	Interferometric surface analysis	[N/A]
Atomic force microscopy	Atomic structure analysis	[28,33,35]
Transmission electron microscopy	Atomic structure analysis	[36,39]
Scanning electron microscopy	Surface imaging, observation	[37,39]
Phosphorus-31 nuclear magnetic resonance	Quantitative structural analysis	[28]
Raman spectroscopy	Chemical structure analysis	[38,54]

known alternatives presented in **Table 6**, because of its sensitivity, cheap implementation, and real-time non-destructive monitoring.

Acknowledgements

Financial support of these studies by the 10/2022/IDUB/II.2 under the Scandium Baltic Region Research Grants—EIRU program is gratefully acknowledged. This study was funded in part by Ministry of Education and Science under project NdS/551425/2022/2022. The support by the DS Programs of Faculty of Electronics, Telecommunications and Informatics, Gdańsk University of Technology, as well as the support by the DS Programs of Faculty of Telecommunications, Computer Science and Electrical Engineering of Bydgoszcz University of Science and Technology are acknowledged.

Conflict of Interest

The authors declare no conflict of interest.

Author Contributions

M.S. and P.J.: conceptualization; M.S. and P.J.: methodology; P.J.: samples preparation; M.C.: SEM measurements, P.J.: SEM analysis and visualization, M.S.: Raman measurements and visualization, P.J.: Raman spectra analysis, M.C.: XPS measurements and visualization, P.J. and M.C.: XPS analysis, M.S.: optical measurements; M.K., J.G., and M.S..: optical measurement data processing and analysis; J.G.: photonic measurements modeling, M.K. and J.G.: visualization; M.K., P.J., and M.S.: writing—original draft preparation; M.K., P.J., and M.S.: writing—review and editing. All authors have read and agreed to the published version of the manuscript.

Data Availability Statement

The data that support the findings of this study are available from the corresponding author upon reasonable request.

Keywords

few-layer black phosphorus, phosphorene, degradation, photonic measurements, interferometer

Received: October 28, 2022
Revised: January 30, 2023
Published online: March 28, 2023

[1] D. Tyagi, H. Wang, W. Huang, L. Hu, Y. Tang, Z. Guo, Z. Ouyang, H. Zhang, *Nanoscale* **2020**, *12*, 3535.
[2] B. Wang, Y. Gu, L. Chen, L. Ji, H. Zhu, Q. Sun, *Nanotechnology* **2022**, *33*, 252001.
[3] C. W. Lee, J. M. Suh, H. W. Jang, *Front. Chem.* **2019**, *7*, 708.
[4] S. Adomavičiūtė-Grabusovė, S. Ramanavičius, A. Popov, V. Šablinskas, O. Gogotsi, A. Ramanavičius, *Chemosensors* **2021**, *9*, 223.
[5] D. Akinwande, N. Petrone, J. Hone, *Nat. Commun.* **2014**, *5*, 5678.
[6] N. R. Glavin, C. Muratore, M. Snure, *Oxford Open Mater. Sci.* **2021**, *1*, 002.
[7] M. Long, P. Wang, H. Fang, W. Hu, *Adv. Funct. Mater.* **2019**, *29*, 1803807.
[8] C. Chakraborty, N. Vamivakas, D. Englund, *Nanophotonics* **2019**, *8*, 2017.
[9] L. Wang, K.-W. Ang, in *2D Materials for Photonic and Optoelectronic Applications*, (Eds.: Q. Bao, H. Y. Hoh), Woodhead Publishing, **2020**, pp. 117–158.
[10] Y. Liu, X. Peng, *Appl. Mater. Today* **2017**, *8*, 104.
[11] N. R. Glavin, R. Rao, V. Varshney, E. Bianco, A. Apte, A. Roy, E. Ringe, P. M. Ajayan, *Adv. Mater.* **2020**, *32*, 1904302.
[12] A. V. Pradeep, S. V. Satya Prasad, L. V. Suryam, P. Prasanna Kumari, *Mater Today Proc* **2019**, *19*, 380.
[13] V. Shanmugam, R. A. Mensah, K. Babu, S. Gawusu, A. Chanda, Y. Tu, R. E. Neisiany, M. Försth, G. Sas, O. Das, *Part. Part. Syst. Charact.* **2022**, *39*, 2200031.
[14] S. Yu, X. Wu, Y. Wang, X. Guo, L. Tong, *Adv. Mater.* **2017**, *29*, 1606128.
[15] S. Ramanavicius, A. Ramanavicius, *Int. J. Mol. Sci.* **2020**, *21*, 9224.
[16] J. Cheng, L. Gao, T. Li, S. Mei, C. Wang, B. Wen, W. Huang, C. Li, G. Zheng, H. Wang, H. Zhang, *Nano-Micro Lett.* **2020**, *12*, 179.
[17] H. Liu, A. T. Neal, Z. Zhu, Z. Luo, X. Xu, D. Tománek, P. D. Ye, *ACS Nano* **2014**, *8*, 4033.
[18] S. Kuriakose, T. Ahmed, S. Balendhran, G. E. Collis, V. Bansal, I. Aharonovich, S. Sriram, M. Bhaskaran, S. Walia, *Appl Mater Today* **2018**, *12*, 244.
[19] S. Das, W. Zhang, M. Demarteau, A. Hoffmann, M. Dubey, A. Roelofs, *Nano Lett.* **2014**, *14*, 5733.
[20] V. Musle, S. Choudhary, *Opt. Quantum Electron.* **2018**, *50*, 285.
[21] V. Tran, R. Soklaski, Y. Liang, L. Yang, *Phys. Rev. B* **2014**, *89*, 235319.
[22] Q. Guo, A. Pospischil, M. Bhuiyan, H. Jiang, H. Tian, D. Farmer, B. Deng, C. Li, S.-J. Han, H. Wang, Q. Xia, T.-P. Ma, T. Mueller, F. Xia, *Nano Lett.* **2016**, *16*, 4648.
[23] X. Yu, S. Zhang, H. Zeng, Q. J. Wang, *Nano Energy* **2016**, *25*, 34.
[24] J. Wang, Y. Jiang, *Eur. Phys. J. D* **2019**, *73*, 255.
[25] W. Shen, C. Hu, S. Huo, Z. Sun, S. Fan, J. Liu, X. Hu, *Opt. Lett.* **2018**, *43*, 1255.
[26] W. Li, Z. Wang, F. Zhao, M. Li, X. Gao, Y. Zhao, J. Wang, J. Zhou, Y. Hu, Q. Xiao, X. Cui, M. J. Eslamibidgoli, M. H. Eikerling, R. Li, F. Brandys, R. Divigalpitiya, T.-K. Sham, X. Sun, *Chem. Mater.* **2020**, *32*, 1272.
[27] M. T. Edmonds, A. Tadich, A. Carvalho, A. Ziletti, K. M. O'donnell, S. P. Koenig, D. F. Coker, B. Özyilmaz, A. H. C. Neto, M. S. Fuhrer, *ACS Appl. Mater. Interfaces* **2015**, *7*, 14557.
[28] Y. Wang, B. Yang, B. Wan, X. Xi, Z. Zeng, E. Liu, G. Wu, Z. Liu, W. Wang, *2D Mater.* **2016**, *3*, 035025.
[29] G. Wang, R. Pandey, S. P. Karna, *Nanoscale* **2015**, *7*, 524.
[30] J.-S. Kim, Y. Liu, W. Zhu, S. Kim, D. Wu, L. Tao, A. Dodabalapur, K. Lai, D. Akinwande, *Sci. Rep.* **2015**, *5*, 8989.
[31] G. Wang, W. J. Slough, R. Pandey, S. P. Karna, *2D Mater.* **2016**, *3*, 025011.
[32] M. van Druenen, *Adv. Mater. Interfaces* **2020**, *7*, 2001102.
[33] S. Kuriakose, T. Ahmed, S. Balendhran, V. Bansal, S. Sriram, M. Bhaskaran, S. Walia, *2D Mater.* **2018**, *5*, 032001.
[34] S. Walia, Y. Sabri, T. Ahmed, M. R. Field, R. Ramanathan, A. Arash, S. K. Bhargava, S. Sriram, M. Bhaskaran, V. Bansal, S. Balendhran, *2D Mater.* **2016**, *4*, 015025.
[35] C. Hyun, J. H. Kim, J.-Y. Lee, G.-H. Lee, K. S. Kim, *RSC Adv.* **2019**, *10*, 350.
[36] A. E. Naclerio, D. N. Zakharov, J. Kumar, B. Rogers, C. L. Pint, M. Shrivastava, P. R. Kidambi, *ACS Appl. Mater. Interfaces* **2020**, *12*, 15844.
[37] S. Su, B. Xu, J. Ding, H. Yu, *New J. Chem.* **2019**, *43*, 19365.
[38] S. Liang, M. Hasan, J.-H. Seo, *Nanomaterials* **2019**, *9*, 566.
[39] A. Favron, E. Gaufrès, F. Fossard, P. L'evesque, A.-L. Phaneuf-L'Heureux, N. Tang, A. Loiseau, R. Leonelli, S. Francoeur, R. Martel, arXiv: Mesoscale and Nanoscale Physics **2014**.
[40] F. Xu, D. Ren, X. Shi, C. Li, W. Lu, L. Lu, L. Lu, B. Yu, *Opt. Lett.* **2012**, *37*, 133.
[41] J. Zhang, et al., *IEEE Photonics J* **2018**, *10*, https://ieeexplore.ieee.org/document/8435931.
[42] S. Gao, W. Zhang, Z.-Y. Bai, H. Zhang, W. Lin, L. Wang, J. Li, *J. Lightwave Technol.* **2014**, *32*, 1682.
[43] F. Zhou, W. Duan, X. Li, J.-T. Tsai, M. B. G. Jun, *J. Manuf. Process.* **2021**, *68*, 180.
[44] Q. Yu, X. Zhou, *Photonic Sens.* **2011**, *1*, 72.
[45] S. Rana, A. Fleming, H. Subbaraman, N. Kandadai, *Opt. Express* **2022**, *30*, 15659.
[46] R. Martinez-Manuel, J. Esquivel-Hernandez, S. Larochelle, *IEEE Sens. J.* **2022**, *22*, 9433.
[47] M. Kosowska, P. Jakóbczyk, M. Rycewicz, A. Vitkin, M. Szczerska, *Sci. Rep.* **2021**, *11*, 12600.
[48] M. Szczerska, M. Kosowska, P. Listewnik, M. Rycewicz, M. Bechelany, Y. Fleger, D. Fixler, P. Jakóbczyk, *Measurement* **2022**, *189*, 110495.
[49] P. Jakóbczyk, M. Kowalski, M. Brodowski, A. Dettlaff, B. Dec, D. Nidzworski, J. Ryl, T. Ossowski, R. Bogdanowicz, *Appl. Surf. Sci.* **2021**, *539*, 148286.
[50] P. Listewnik, M. Szczerska, P. Jakóbczyk, *Mater. Res. Express* **2021**, *8*, 065004.
[51] G. D. Khattak, A. Mekki, L. E. Wenger, *J. Non-Cryst. Solids* **2009**, *355*, 2148.
[52] J. Pang, A. Bachmatiuk, Y. Yin, B. Trzebicka, L. Zhao, L. Fu, R. G. Mendes, T. Gemming, Z. Liu, M. H. Rummeli, *Adv. Energy Mater.* **2018**, *8*, 1702093.
[53] A. Dettlaff, G. Skowierzak, L. Macewicz, M. Sobaszek, J. Karczewski, M. Sawczak, J. Ryl, T. Ossowski, R. Bogdanowicz, *J. Phys. Chem. C* **2019**, *123*, 20233.
[54] H. B. Ribeiro, M. A. Pimenta, C. J. S. De Matos, *J. Raman Spectrosc.* **2018**, *49*, 76.
[55] J. Kumar, et al., in *2020 IEEE International Reliability Physics Symposium (IRPS)*, IEEE, Dallas, TX, USA **2020**, https://www.proceedings.com/54980.html.

[56] M. Kosowska, D. Majchrowicz, K. J. Sankaran, M. Ficek, K. Haenen, M. Szczerska, *Materials* **2019**, *12*, https://doi.org/10.3390/ma12132124.
[57] D. Majchrowicz, M. Hirsch, P. Wierzba, M. Bechelany, R. Viter, M. Jedrzejewska-Szczerska, *Sensors* **2016**, *16*, 416.
[58] S. Zhang, X. Zhang, L. Lei, X.-F. Yu, J. Chen, C. Ma, F. Wu, Q. Zhao, B. Xing, *Angew. Chem., Int. Ed.* **2019**, *58*, 467.
[59] M. Bredol, D. Leers, L. Bosselaar, M. Hutjens, *J. Lightwave Technol.* **1990**, *8*, 1536.
[60] S. P. Koenig, R. A. Doganov, H. Schmidt, A. H. Castro Neto, B. Özyilmaz, *Appl. Phys. Lett.* **2014**, *104*, 103106.
[61] A. Wieloszynska, Ł. Macewicz, P. Jakobczyk, K. Pyrchla, R. Bogdanowicz, in *Frontiers in Optics + Laser Science APS/DLS JTu3A*, OSA, Washington, DC **2019**, Vol. *18*.